Performance of MIMO systems based on dual-polarized antennas in urban microcellular environments

Jesús Pérez, Jesús Ibáñez, Luis Vielva, and Ignacio Santamaría
University of Cantabria
Email: jperez@gtas.dicom.unican.es

***Abstract*— Recent works have analyzed the potential performance of MIMO systems using dual-polarized antennas at both ends of the wireless link. These works assume Rayleigh and Ricean fading MIMO channel models. Here, we analyze the capacity of such systems in microcellular environments using a physical model of the MIMO channel. The use of a physical model permits us to analyze the impact of environmental parameters, like antennas location and orientation, on the system performance. As example, we present ergodic and outage capacity estimations in a specific urban environment from the predictions of a site-specific ray-tracing propagation tool.**

I. Introduction

The conventional MIMO systems use multiple element array antennas at both ends of the wireless link. To exploit the potential benefits of MIMO systems in outdoor environments the spacing between antennas must be large enough to avoid high spatial correlation. But in small microcells and picocells, the available space uses to be limited. A simple and compact alternative to conventional MIMO systems is to use dual-polarized antennas at transmitter (Tx) and receiver (Rx). In this case, using a single antenna at both ends of the wireless link, a 2x2 MIMO configuration is obtained. Recent works have analyzed the potential performance of such systems in terms of capacity [1] or bit error rate (BER) for different coding techniques as Spatial Multiplexing and Space-Time Block coding [2], [3]. These works are based on Rayleigh and Ricean fading MIMO channel models.

In this paper we analyze the ergodic and outage capacity of such MIMO configurations, in urban microcellular environments, using a physical model of the MIMO channel. It permits us to estimate the system capacity in specific environments and antennas locations, as well as to analyze how the specific antennas characteristics (radiation pattern, polarization characteristics, cross-polarization discrimination) have influence on the system performance.

The paper is organised as follows: In section II we describe the physical modelling of the MIMO channel. The characterization of the system performance, in terms of ergodic and outage capacity, is presented in section III. Finally, section IV shows simulation results in a specific microcellular environment for specific antennas.

II. MIMO Channel Model

The channel is assumed to be flat over the frequency band and quasi-stationary. Under such assumptions the channel matrix, for a given realization of the MIMO channel, can be expressed as follows

$$\mathbf{H} = \begin{bmatrix} h_{11} & h_{12} \\ h_{21} & h_{22} \end{bmatrix}, \tag{1}$$

where the diagonal elements of $\mathbf{H}$ correspond to transmission and reception on the same polarization, while the off-diagonal entries correspond to transmission and reception on orthogonal polarizations. Each entry of $\mathbf{H}$ is the complex envelope of the channel response for the corresponding polarization branches of the Tx and Rx antennas. They are modelled as the superposition of a number of uniform plane waves due to the multi-path propagation

$$h_{ij} = \sum_{n=1}^{N} V_n^{ij} \exp(j\phi_n), \quad V_n^{ij} = \mathbf{E}_n^j \cdot \mathbf{a}^i(\theta_n, \phi_n), \tag{2}$$

where N is the number of multipath waves reaching the Rx, $\mathbf{E}_n^j$ is the electric field of the n-th wave at the Rx, when the j-th polarization branch of the Tx antenna is transmitting, and $\mathbf{a}^i$ is the polarization vector [4] of the Rx antenna for the i-th polarization branch. θ_n and ϕ_n represent the propagation direction of the n-th incoming wave, referred to the local spherical coordinate system of the Rx antenna. In general, $\mathbf{a}_n^i$ is a complex vector which fully determines the radiation and polarization characteristics of the Rx antenna at the i-th polarization branch. It is usually referred to a given local spherical coordinate associated to the antenna

$$\mathbf{a}^i(\theta, \phi) = E_\theta^i(\theta, \phi)\,\hat{\theta}_a + E_\phi^i(\theta, \phi)\,\hat{\phi}_a \tag{3}$$

Note that for a given incident wave $\mathbf{E}_n^j$, the specific orientation of the Rx antenna can have a significant influence on the amplitude of the multipath terms V_n^{ij}, and therefore on MIMO channel elements h_{ij}.

The E-field of each incoming wave at the Rx antenna ($\mathbf{E}_n^j$) is obtained from a 3-D site-specific ray-tracing propagation model taking into account the radiation and polarization characteristics of the Tx antenna, as well as the specific characteristics of the propagation scenario. The propagation

0-7803-8521-7/04/$20.00 © 2004 IEEE

model is based on the Geometric Theory of Diffraction (GTD/UTD) considering multiple reflections off ground and buildings, as well as diffractions around the building wedges of the scenario [5]. The model requires a detailed description of the environment, which includes geometric and electromagnetic properties of the elements of the propagation scenario: ground and buildings. The propagation model also requires as input the location, orientation, polarization and radiation characteristics of the Tx antenna as well as the location of the Rx. The GTD/UTD model provides the waves reaching the Rx with the associated E-fields ($\mathbf{E}_n^j$ in (2)). Detailed information about the propagation model and about other similar models can be found in [5], [6] and [7].

Then, the V_n^{ij} terms in (2) are complex values that directly depend on the antennas and on the physical characteristics of the propagation scenario through reflections, diffractions and scattering of the multi-path waves. We assume that the wave phases ϕ_n in (2) are uniformly distributed uncorrelated random variables [8], [9]. This assumption leads to a stochastic model of the MIMO channel.

The potential correlations between the channel matrix entries are implicitly considered by the propagation model as function of the propagation environment, as well as the radiation and polarization characteristics of the antennas. For example. the cross-polarization discrimination (XPD) of the antennas has a significant influence on the correlation between the channel matrix entries.

A. Channel normalization

The propagation model predicts both the large-scale fading and the small-scale fading. To get further insight into the effects of the small-scale fading, we can normalize the channel matrix, removing the average path-loss

$$\mathbf{H}_{norm} = \frac{1}{\sqrt{\alpha}}\mathbf{H}, \tag{4}$$

where α represents the average path-loss. It can be expressed as follows

$$\alpha = \frac{1}{4}E\left[||\mathbf{H}||_F^2\right], \tag{5}$$

being $||\mathbf{H}||_F^2$ the squared Frobenius norm of the channel matrix realizations. After the channel normalization the average received power at each polarization branch equals the total transmitted power E_s, so the signal-to-noise ratio (SNR) will be

$$\rho = E_s/\sigma_n^2, \tag{6}$$

being σ_n^2 the noise power at the polarization branches of the Rx antenna.

III. Ergodic and Outage Capacity

We assume that the channel matrix is known at the Rx, but unknown at the Tx. We also assume that the transmitted signals are independent and equi-powered at the polarization branches of the Tx antenna. Then, for a given realization of the channel, the capacity (in bps/Hz) will be given by [10]

$$C = \log_2 \det\left(I_2 + \frac{\rho}{2}\mathbf{H}\mathbf{H}^H\right), \tag{7}$$

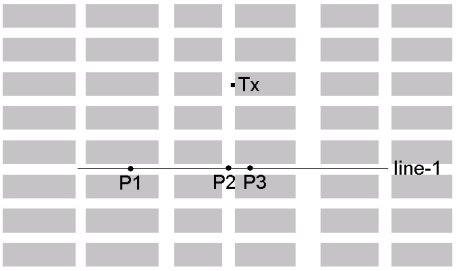

Fig. 1. Top view of the propagation scenario showing the Tx antenna position. The points P1, P2 and P3 and the line-1 shows the Rx antenna locations in the simulations.

where I_2 is the 2×2 identity matrix, ρ is the SNR at the polarization branches of the Rx antenna, $\mathbf{H}$ is a matrix channel realization and the superscript $(\cdot)^H$ represents the hermitian operator. The ergodic capacity is the ensemble average of the capacity for all the realizations of the MIMO channel: $E[C]$.

Usually, the outage capacity is used to characterized the statistical distribution of the capacity [11], [10]. The $q\%$-outage capacity (C_{out}) is defined as the information rate that is guaranteed for $1 - q/100$ of the channel realizations. It can be mathematically expressed as follows

$$P\left(C \leq C_{out}\right) = q/100. \tag{8}$$

The following section shows ergodic and outage capacity simulation results in specific scenarios as function of the SNR and the Rx location.

IV. Simulation Results

The method described above can be used to estimate the ergodic and outage capacity in any micro- or pico-cellular scenario and for any type of antennas and polarization scheme. As an example, fig.1 shows a top view of a micro-cellular scenario consisting of 48 regularly distributed buildings with uniform height (25m) and rectangular section, forming a rectilinear grid of parallel and perpendicular streets. This scenario is an area of the midtown Manhattan which has been used for the validation of propagation models in urban micro-cells [6], [7]. The rooftops are assumed to be flat. The radio-propagation through the buildings is neglected. The area of the environment is 900 x 500 m2. The Tx antenna is located of 20 m height on a building wall. The Rx antenna is always 1.5 m height. We assume that both Tx and Rx antennas are omnidirectional in amplitude and phase. We also assume that both antennas are dual-linearly polarized and they are vertically oriented. All the simulations have been carried out at 1.8 GHz.

In all the simulations there were more than 10 multipath waves reaching the Rx antenna, being the average number of rays around 100 and 20 in LOS (line-of-sight) and NLOS (non-line-of-sight) points, respectively. Due to the random nature of the MIMO channel model, the capacity results have been obtained from MonteCarlo simulation.

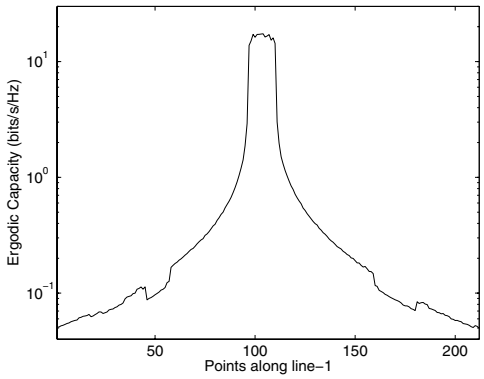

Fig. 2. Normalized ergodic capacity along line-1 of fig.1 without channel normalization

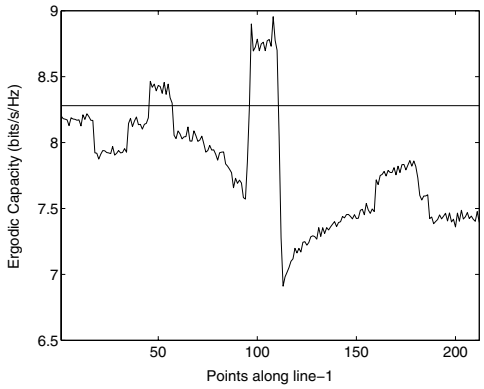

Fig. 3. Ergodic capacity along line-1 of fig.1

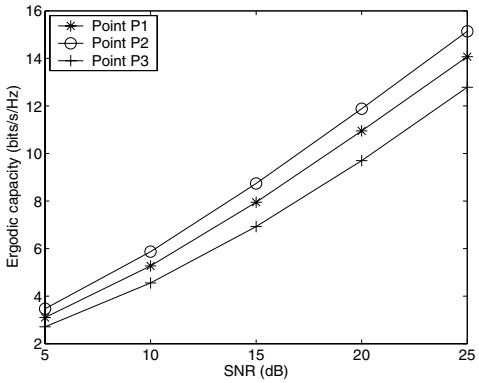

Fig. 4. Ergodic capacity at the points P1, P2 and P3 of fig.1 as a function of the SNR

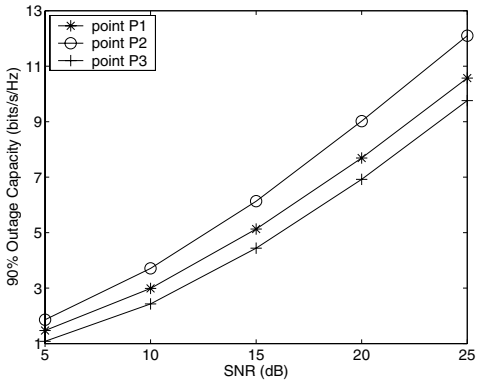

Fig. 5. 90% outage capacity at the points P1, P2 and P3 of fig.1 as a function of the SNR

A. Ergodic capacity without channel normalization

Fig. 3 shows the simulated ergodic capacity for a fixed Tx antenna location and variable Rx position along line-1 (see fig.1). Both, the Tx and the Rx antennas have perfect XPD. The average path-loss at the Rx locations is 15 dB. The channel matrix is not normalized so the effect of the large-scale fading in included in the simulations. The graph shows that, in absence of channel normalization, the capacity values are mainly determined by the path-loss at the receiver locations. Hereafter we will assume normalized channel matrix in all the simulation results.

B. Comparison between LOS and NLOS situations

Fig. 3 shows the simulated ergodic capacity for a normalized channel along the points of line-1. Now, only the effect of the small-scale fading is included in the capacity curves. The SNR at the Rx polarization branches is always 15 dB. As before, both the Tx and the Rx antennas have perfect XPD. As it is expected, the capacity increases significantly when passing from NLOS to LOS points. The curve also shows the significant variations of the capacity at NLOS points as a function of the Rx antenna location. As reference, the horizontal line shows the ergodic capacity for an uncorrelated Rayleigh MIMO channel.

C. Capacity as a function of the SNR

Figures 4 and 5 shows the ergodic and 90%-outage capacity as a function of the SNR at the Rx antenna, when the Rx antenna is located at the points P1, P2 and P3 of fig.1. We assume antennas with perfect XPD and normalized channel. Significant differences can be observed among the different locations of the Rx antenna. The points P1 and P3 are NLOS locations and P2 is a LOS site. The number of waves reaching P1, P2 and P3 were 20, 196 and 24, respectively.

D. Antennas with finite XPD

Fig. 6 shows the ergodic capacity obtained along line-1 when the Tx antenna XPD equals ∞ and 10 dB. The SNR at the Rx polarization branches is 15 dB. As it is expected, lower antenna XPD produces higher correlation in transmission and therefore lower capacity. The XPD introduces a nearly constant shift in the ergodic capacity. This behaviour occurs both at LOS and NLOS locations of the receiver.

E. Capacity along parallel streets

Fig. 7 shows the simulated ergodic capacity along lines parallel to line-1 but at different streets. As before, the SNR at the Rx polarization branches is 15 dB. The curves are similar because of the symmetry of the environment. No significant differences are observed for different parallel streets.

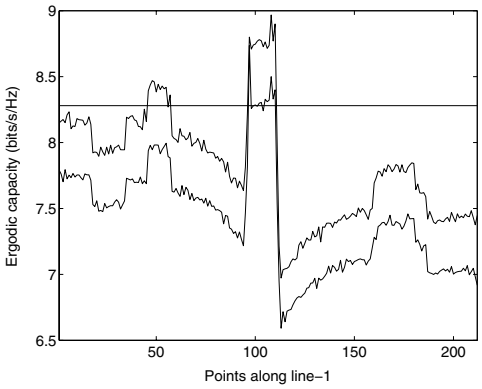

Fig. 6. Ergodic capacity along line-1 of fig.1 when the XPD of the Tx antenna is ∞ and 10 dB

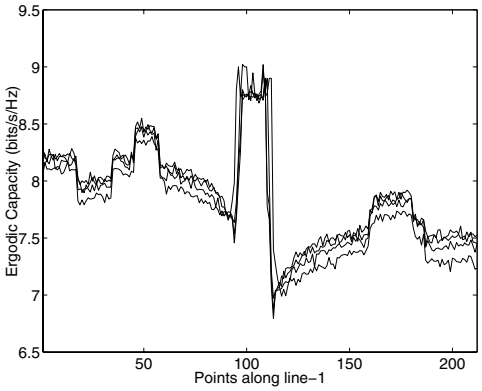

Fig. 7. Ergodic capacity along streets parallel to line-1 of fig.1

V. Conclusions

We have used a physical channel model to estimate the capacity of MIMO systems, based on two dual-polarized antennas, in urban micro-cellular environments. A site-specific propagation model provides the amplitude of the multi-path waves at the receiver. The phases of the multi-path waves are assumed to be uncorrelated uniform random variables. The use of a physical channel model permits us to estimate the MIMO channel capacity in specific scenarios and to study the dependency of the capacity on the antennas location and radiation and polarization characteristics . As an example, we have analyzed the ergodic capacity in a typical urban micro-cellular scenario characterized by uniform building forming a rectangular grid of parallel and perpendicular streets. The antennas were dual-linear polarized and vertically oriented. We have obtained some conclusions specific of this type of environment.

The simulated results show that when the large-scale fading is included in the simulations, the ergodic capacity is mainly determined by the path-loss at the Rx locations. When only the small-scale fading is considered significant variations of the capacity can be observed as a function of the Rx location. In general, the capacity at LOS points is higher than in a NLOS points. The capacity at NLOS points shows significant variations along a street. The XPD of the antennas has important influence on the capacity. In general, higher antenna XPD leads to higher capacity values. The capacity values do not change meaningfully along parallels streets. It is important to note that some of the above conclusions are specific of this type of propagation environment and can not be directly generalized to other micro-cells. In any case, the method presented can be used to estimate the capacity in specific microcells as well as to study the impact of the environment and antenna characteristics in the performance of such MIMO systems.

Acknowledgment

This work has been partially supported by Spanish Ministry of Science and Technology under project TIC2001-0751-C04-03.

References

[1] A. Paulraj, R. Nabar, and D. Gore, *Introduction to Space-Time Wireless Communications*. Cambridge University Press, 2003.

[2] R. U. Nabar, H. Bolcskei, V. Erceg, D. Gesbert, and A. J. Paulraj, "Performance of multiantenna signaling techniques in the presence of polarization diversity," *IEEE Transactions on Signal Processing*, vol. 50, pp. 2553–2562, October 2002.

[3] H. Bolcskei, R. U. Nabar, V. Erceg, D. Gesbert, and A. J. Paulraj, "Performance of spatial multiplexing in the presence of polarization diversity," in *Proc. IEEE International Conference on Acoustics, Speech, and Signal Processing*, vol. 4, Salt Lake City, UT, May 2001, pp. 2437–2440.

[4] C. A. Balanis, *Antenna Theory. Analysis and Design*. John Wiley and Sons, 1997.

[5] M. F. Cátedra and J. Pérez, *Cell Planning for Wireless Communications*. Norwood, MA: Artech House, 1999.

[6] S. Y. Tan and H. S. Tan, "A microcellular communications propagation model based on the uniform theory of diffraction and multiple image theory," *IEEE Transactions on Antennas and Propagation*, vol. 44, pp. 1317–1326, October 1996.

[7] V. Erceg, S. J. Fortune, J. Ling, A. J. Rustako, and R. A. Valenzuela, "Comparison of computer-based propagation prediction tool with experimental data collected in urban microcellular environments," *IEEE Journal on Selected Areas in Communications*, vol. 15, pp. 677–684, May 1997.

[8] G. D. Durgin, *Space-Time Wireless Channels*. Upper Saddle River, NJ: Prentice Hall PTR, 2003.

[9] H. Zhu, J. Takada, K. Araki, and T. Kobayashi, "A random-phase-assisted ray-tracing code for wireless channel modeling," *Applied Computational Electromagnetic Society Journal*, vol. 16, pp. 69–78, March 2001.

[10] I. E. Telatar, "Capacity of multi-antenna gaussian channels," *European Transaction on Telecommunications*, vol. 10, pp. 585–595, November/December 1999.

[11] E. Biglieri, J. Proakis, and S. Shamai, "Fading channels: Information-theoretic and communications aspects," *IEEE Transactions on Information Theory*, vol. 44, pp. 2619–2692, October 1998.